



A theoretical and experimental study on L-tyrosine and citrate mediated sustainable production of near infrared absorbing twisted gold nanorods



Anshuman Jakhmola^{a,*¹}, Raffaele Vecchione^{a,b,**¹}, Valentina Onesto^a, Francesco Gentile^d, Martina Profeta^a, Edmondo Battista^{a,b}, Anastasios C. Manikas^a, Paolo A. Netti^{a,b,c}

^a Istituto Italiano di Tecnologia, IIT@CRIB, Largo Barsanti e Matteucci 53, 80125 Napoli, Italy

^b Centro di Ricerca Interdipartimentale sui Biomateriali CRIB, Università di Napoli Federico II, Piazzale Tecchio 80, 80125 Napoli, Italy

^c Dipartimento di Ingegneria Chimica, dei Materiali e della Produzione Industriale, Università di Napoli Federico II, Piazzale Tecchio 80, 80125 Napoli, Italy

^d Dipartimento di Ingegneria Elettrica e delle Tecnologie dell'Informazione, Università degli Studi di Napoli Federico II, Via Claudio, 21, 80125 Napoli, Italy

ARTICLE INFO

Keywords:

Twisted gold nanorods
Biomolecules
Green synthesis
SERS
Photothermal therapy

ABSTRACT

Anisotropic gold nanoparticles displaying plasmon band in the near infrared region can play a crucial role in cancer therapy particularly with techniques such as photothermal therapy (PTT) and photodynamic therapy (PDT). Herein, we report an efficient, sustainable, one pot protocol for the fabrication of an unusual gold anisotropic shape, which we have named as twisted gold nanorods. These particles, though having dimensions in the nanoscale regime comparable to those of gold nanorods, display a continuous flat plasmon band like that of 2-D gold nanowire networks, extended up to the NIR-III (SWIR) range. The proposed strategy is simple and does not require any seed mediation, heating or potential toxic templates or organic solvents. Our process is based on the slow reduction of gold salt in presence of two mild reducing agents viz. L-tyrosine (an amino acid) and trisodium citrate. We observed that when both molecules are present together in particular concentrations, they direct the growth in form of twisted gold nanorods. The mechanism of growth has been described by a Diffusion Limited Aggregation numerical scheme, where it was assumed that both L-tyrosine and the gold ions in solution undergo a stochastic Brownian motion. The predictions of the model matched with the experiments with a good accuracy, indicating that the initial hypothesis is correct. The final structure has been thoroughly characterized in terms of morphology, while SERS and cytotoxic activity have also been demonstrated.

1. Introduction

Nanotechnology is a priority field for today's innovation leaders and it is on the verge of revolutionizing many technologies and industry sectors. Using nanoscience a variety of novel materials like quantum dots [1], metal/alloy oxides [2], metal organic framework (MOF) [3–5], mesoporous materials [6] have been developed in the past decades which have displayed fantastic properties. Among all others, gold nanomaterials are favored by scientists and are still the most studied because of their unique size- and shape-dependent optical and electronic properties [7]. Over the past two decades research investigations have been focused and shifted more towards anisotropic gold nanostructures which have found breakthroughs in numerous new applications, particularly in the fields related to nanomedicine [8], medical

diagnostics [9], virus detection [10], photothermal therapy [11], photoacoustic imaging [12], and X-ray computed tomography [13]. Anisotropic gold nanoparticles hold some unique physico-chemical properties which are absent in the spherical geometry and arise due to the presence of asymmetric axes which give rise to shape-specific interesting properties [14]. One of the most important properties is the development of a plasmon band in the NIR region because absorption of biological tissue is low in this region. This biological transparency makes them an important asset for cancer photo-thermal therapy. Among various anisotropic gold nanostructures, unidimensional shapes such as rods [15], ribbons [16], wires [17,18], display plasmonic resonance in the NIR region and have therefore attracted worldwide interest. Their design and development considerably accelerated in the last decade after the development of the seed mediated wet chemical

* Corresponding author.

** Correspondence to: R. Vecchione, Centro di Ricerca Interdipartimentale sui Biomateriali CRIB, Università di Napoli Federico II, Piazzale Tecchio, 80, 80125 Napoli, Italy.

E-mail addresses: anshumanjakhmola@bellsouth.net (A. Jakhmola), raffaele.vecchione@iit.it (R. Vecchione).

¹ These authors have contributed equally to this work.

protocol [19] which provided intriguing strategies for the synthesis of various types of anisotropic nanostructures [14]. In particular, seed-mediated methods facilitate the growth of seed particles by using some rigid templates, molecules or surfactants in a step by step way, so that it becomes easier to control the growth in a particular direction. The best example of such a molecule is hexadecyltrimethylammonium bromide (CTAB) which is one of the most versatile molecules in the synthesis of anisotropic gold nanoparticles [20] including gold nanorods, and nanowires [14,21]. This molecule is now used for the commercial synthesis of gold nanorods of various aspect ratios [22]. However, CTAB is a toxic molecule, which needs a tedious protocol to be removed from the gold surface when employed in applications related to biotechnology and nanomedicine [23]. More eco-friendly alternative approaches are now being designed which make use of simple biomolecules or biocompatible polymers, such as amino acids [24], peptides [25], PVP [26], and plant extracts mimicking bio-inspired material synthesis as found in natural world [27]. These are generally non-toxic and biodegradable, but they have weak control over particle size, distribution and shape, maybe due to their simple structure and small size. Another approach consists in designing special peptides or protein molecules which provide at the same time improved biocompatibility and solubility [28,29]. In a recent article small sequence peptide chains were used to synthesize gold nanoribbons [30]. However, designing special peptide sequences is a tedious multi-step costly process, requiring a variety of organic solvents and the final yield of pure molecule is quite low after purification.

In this article, we present a very simple and convenient protocol to obtain a unique-shaped anisotropic gold structure that we have named as twisted gold nanorods as they are cylindrical and have lengths of few tens of nanometers like that of nanorods but have random twists, turns, kinks and curves along their lengths. The protocol requires two simple biomolecules viz. L-tyrosine and trisodium citrate as reducing agents. To the best of our knowledge, this shape has not been mentioned in the literature so far. In a previous article, Wang et al. reported the formation of similar gold nanostructures along with gold nanowire network by laser ablation method [31]. The two structures were separated from each other by simple filtration. However, the final product lacked homogeneity and looked more like broken nanowire networks. In literature there are also other similar structures like nanodumbbells [32], nanokites [33], nanotadpoles [17], crooked gold nanorods [34]; however, most of them required high temperatures, radiation, toxic chemicals, or a two-step seeded approach. A comparison with these structures has been shown in Table 2 in Supplementary data. Previously, we have also demonstrated the formation of gold nanoflowers and quasi-spherical gold nanoparticles using exactly the same reagents [24]. Here, we have further extended our work on chemistry and theoretical simulations (cellular automata and diffusion limited aggregation (DLA) simulations) to demonstrate the effect of the amount L-tyrosine molecules and sequence of addition on the final morphology of particles [24]. Once dealing with nanomaterials meant for *in vivo* applications, NIR-II (~1000 to 1350 nm) is recognized to offer more tissue penetration than simple NIR (~700 to 1000 nm) thus it can find diverse bio and photothermal applications [35,36], a burning topic in nanomedicine. However, photo-thermal agents within NIR-II are still rare [37]. Moreover, the continuous band, which makes their use more flexible, is observed only in the nanowire network (NWNs) type 2-D structure of gold but it is difficult to use NWNs in nanomedicine as one of their axes can extend up to tens of micrometer. The advantages of nanocrystals having broad absorption profiles over nanorods was recently cited in an article [37]. The authors designed raspberry shaped gold nanoparticles having a broad absorption profile, which extended up to NIR-II region. A unique feature of the proposed twisted gold nanorods is that they absorb in NIR-II region and even more surprisingly, the absorbance extends up to NIR-III, also called short-wavelength infrared (SWIR), region (Fig. 1). Additionally, we have also shown some preliminary biological analysis to validate the product in

terms of biosafety by testing their cytotoxicity. Further, we have also demonstrated their applications in the field of surface enhanced Raman spectroscopy (SERS).

2. Experimental

2.1. Materials

Gold (III) chloride trihydrate (99.9%), trisodium citrate dihydrate, L-tyrosine, adenine, 4-mercaptopbenzoic acid (MBA), sodium hydroxide, were purchased from Sigma Aldrich and were used as such. Milli-Q water was used in all the experiments.

2.2. Synthesis of twisted gold nanorods and nanodendrites

The basic principle of synthesis methodology was based on the green protocol already developed in our lab with which we could easily synthesize gold nanowire networks [17], gold foam [17], ultra-small gold particles [38], quasi-spherical gold nanoparticles and particularly gold nanoflowers [24]. In summary, stock solutions of chloroauric acid (4.0 mM), trisodium citrate (38.8 mM) were prepared in milli-Q water while L-tyrosine (10 mg mL⁻¹, 55.2 mM) was prepared in highly alkaline solution as discussed before [24]. However, a few modifications and precautions were necessary to modulate the new shapes. For example, for these new structures the amount of L-tyrosine was reduced to one forth (0.275 mM) as compared to the case of nanoflowers (1.10 mM) [24]. For twisted gold nanorods trisodium citrate was added to auric chloride solution followed by addition of L-tyrosine solution while for gold nanodendrites L-tyrosine was added to auric chloride solution followed by trisodium citrate. The sequence of addition of reactants also played a vital role in modulating the final structure. Since we had already optimized the process as in the case of nanoflowers we did not do any further optimization as reducing the amount of L-tyrosine or increasing the amount of trisodium citrate resulted in the formation of nanowire networks. The final concentrations of reagents in the reaction mixture were, auric chloride (2 mM), trisodium citrate (between 19.4 mM) and L-tyrosine (0.275 mM). The reaction was allowed to proceed for few hours and the solution was then centrifuged at 14000 RPM followed by re-dissolving the pellet in Milli-Q water. This cycle was repeated twice to remove any unreacted reactants.

2.3. Characterization

Gold nanostructures were characterized by transmission electron microscopy (TEM), field emission scanning electron microscopy (FESEM), atomic force microscopy (AFM), and X-ray photoelectron spectroscopy (XPS). TEM images were obtained using a TECNAI 20 G2: FEI COMPANY (CRYO-TEM-TOMOGRAPHY, Eindhoven) with a camera Eagle 2HS. The images were acquired at 200 kV; camera exposure time: 1 s; size 2048 × 2048. SEM images were obtained using Ultraplus Zeiss FESEM. For SEM and energy dispersive X-ray (EDS) measurements, a small drop of solution containing gold nanoflowers was spread onto the surface of a silica wafer and was carefully mounted on an aluminum stub covered by a carbon tape. Sputter coating was not required for the samples and the samples were then placed on the sample holder of the microscope and imaged using 10–20 kV accelerating voltage. Atomic force microscopy, Dimension Icon form Bruker with PeakForce ScanAsyst mode, was used for the characterization of twisted gold nanorods. All measurements were performed in a dry environment over sampling areas of 1 μm × 1 μm and 500 nm × 500 nm. Room temperature was held fixed for all the acquisitions. Ultra-sharp Si probes with a nominal tip radius less than 5 nm were used for achieving high resolution. Multiple measurements were performed in different scan directions to avoid artifacts. At least four images in height mode (trace and retrace) were recorded per each sample. The images had a resolution of 512 × 512 points and were acquired at a scanning rate of

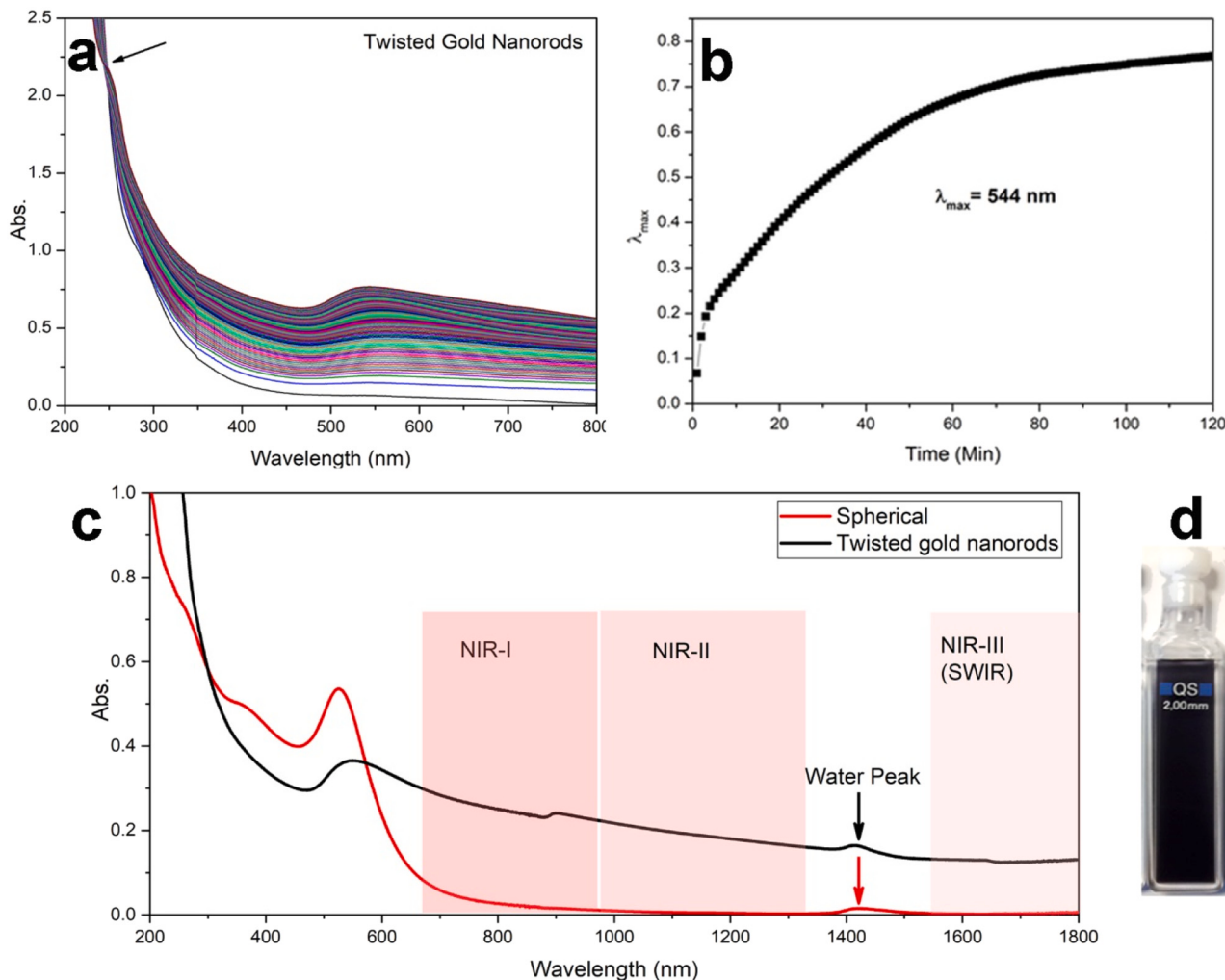


Fig. 1. UV-vis spectra of (a) Time-course UV-vis spectroscopy measurements of twisted gold nanorods; (b) Evolution of peak at 544 nm with time; (c) UV-vis-NIR spectra of twisted gold nanorods (black) displaying different zones in NIR absorbance (NIR I (~700 to 1000 nm) NIR II (~1000 to 1350 nm) and NIR III or SWIR (~1550 to 1870 nm) and spherical particles (red) synthesized by PVP mediated protocol [38] with same amounts of reactants; (d) Black colored colloidal sol of twisted gold nanorods (For (c) 1 mm quartz cuvette and low slit width were used to avoid noise in NIR region). (For interpretation of the references to colour in this figure legend, the reader is referred to the web version of this article.)

1 Hz.

X-Ray Photoelectron spectra were recorded on a XPS Versa Probe II (PHI, Chanhassen US) by large area analysis mode where the monochromatic Al anodic beam of 100 μm , at 100 W power, normal to the surface, is rastered over an area of $1400 \times 300 \mu\text{m}$ with the analyzer fixed at 45° with sample surface. Survey spectra were acquired with an accumulation time of at least 20 min at high pass energy (187 keV) while high resolution spectra of the elements of interests were acquired at a pass energy of 11.7 keV with same power as above and at 0.1 eV resolution. Spectra were analyzed by Multipack (PHI, Chanhassen US) software and all the peaks were referenced to the adventitious carbon peaks C1s at 284.8 eV binding energy. The entire XPS study was carried out on freshly prepared twisted gold nanorods.

2.4. SERS analysis

Gold nanostructures hold unique optical properties and can induce huge enhancement in the Raman scattering (Surface Enhanced Raman Scattering) because of the localized surface plasmons. In our case, we tested the fabricated twisted gold nanorods as SERS active substrates. Adenine and 4-MBA were used as probe molecules and have been widely used in SERS experiments because both adsorb firmly on gold surface (adenine via the amine group and 4-MBA via the sulfur containing on to

the mercapto group) [39]. The samples were prepared by mixing the probe molecules with the gold nanostructures and shaking the mixture on a mechanical shaker for few hours. The solutions were then mixed, in a ratio of 1:1 v/v to a final volume of 100 μl . After mixing 30 μl of the final solution, it was placed on a microscope glass slide covered tightly with aluminum foil. This drop was then analyzed by $10 \times /0.25$ LWD objective after focusing a 780 nm laser line on it.

2.5. Cell culture

To test the biological effect of the nanoparticles, immortalized mouse cerebral endothelial (bEnd.3) cells (American Type Culture Collection, Manassas, VA), were chosen as model cell line. Cells were cultured in DMEM with 4.5 g L^{-1} glucose, supplemented with 10% Fetal Bovine Serum (FBS), 1% glutamine, 1% non-essential amino acids and 100 U mL^{-1} penicillin and 0.1 mg mL^{-1} streptomycin in 100 mm diameter cell culture dish, in a humidified atmosphere at 37°C and 5% CO_2 .

2.6. Cell viability assay

3×10^4 bEnd.3 cells were seeded on 12 wells plate and incubated for 24 h to obtain a sub-confluent monolayer. Cells were then treated with nanoparticles suspension in cell culture medium at a final gold

concentration of 0.2 mM. Prior to cell treatment, nanoparticles suspension was filtered through a 0.2 µm pore-size sterile filter. After a contact time of 24 h, cells were rinsed twice with PBS to remove the non-internalized nanoparticles and cell viability was assessed after 1, 3 and 6 days. Cell survival to nanoparticles treatment was quantified by means of Alamar Blue Assay, according to manufacturer's procedure, at any exposure time. Data were reported as the percentage of viable cells normalized to non-treated cells. All experiments were performed in triplicate.

3. Results and discussion

3.1. Twisted nanorods

Twisted nanorods can be regarded as intermediate structures between 1-D nanostructures like nanorods and 2-D structures like nanowire networks, as on one hand they have a small aspect ratio like nanorods while on other hand their absorption spectrum closely resembles that of nanowire network structures [18,40]. To the best of our knowledge there is no method to synthesize a homogenous colloidal solution of twisted gold nanorods which displays absorption up to SWIR region. Moreover, this shape was achieved by an easy one pot seedless room temperature green method. Specifically, we used the same reagents adopted for the synthesis of gold nanoflowers in our previous article [24], but with a lower amount of L-tyrosine (= one fourth (1/4) of the previous value (0.275 mM)) and adding it after the addition of citrate in the Au³⁺ solution. By making these adjustments the morphology of the final product entirely changed to twisted nanorods [Au³⁺(1) + Trisodium Citrate (2) + L-tyrosine (3)].

After initial mixing of the reagents, the colour of colloidal solution changed from yellow to colorless, indicating the reduction of gold ions. This was followed by a bluish black colour, and finally a black colour sol was formed (Fig. 1d). However, this colloidal solution was stable for months and the sol did not precipitated to form gold foam like in our previous article [17]. The UV-vis-NIR spectra after more than one month displayed hardly any change and the solution remained colloidal in form of a black liquid (see Supplementary data Fig. S1). After the completion of reaction, the UV-vis-NIR spectroscopy measurement displayed a prominent isosbestic point at around 250 nm followed by a small transverse band at 544 nm and a flat absorption profile extending up to SWIR region (Fig. 1 a-c, arrow in 1c is the peak due to absorption of water in the IR region). According to theoretical predictions this flat absorption arises due to superposition of the longitudinal resonance of 1-D gold structures of variable aspect ratios, (Fig. 1a, & c) [17,41]. Very interestingly, the absorption profile extended up to the SWIR region. When the particles were analyzed by TEM, twisted gold nanorods with round tips were found to be formed in high yields. Fig. 2 displays the TEM micrographs at different magnifications of the as synthesized materials. A careful examination revealed their lengths being between 40 and 70 nm with rounded tips and diameters of about 4–8 nm (Fig. 2h). A large percentage of the twisted nanorods were bent with abrupt curvatures and twists. The electron diffraction patterns (SAED) of these twisted nanorods displayed a ringed pattern corresponding to the (111), (200), (220), (311), (420) crystal planes thus confirming a polycrystalline nature with face-centered cubic (fcc) crystals, which indicates that they are formed by fusion of small individual gold nanoparticles (Fig. 2d and Supplementary data Fig. S2). TEM micrographs of early stage of formation of twisted gold nanorods confirms this theory where particle and clumps formation could be clearly observed (Fig. 3c &d). This phenomenon was also observed in the formation of nanowire networks, gold foam and ultra-small gold nanoparticles when reduced with trisodium citrate at room temperature and has been discussed in detail in our previous articles [17,38,42]. SEM studies on this shape was also carried out and displayed clusters of twisted gold nanorods. The EDX analysis displayed peaks corresponding to Au, C, O etc. as expected (see Supplementary data Fig. S3a and S3a2).

3.2. Dendritic gold nanostructures (gold nanodendrites)

Dendritic gold nanostructures can be regarded as gold nanoparticle superstructures which are formed when individual gold nanocrystals self-assemble, grow and organize to form a complex 3-D structure. Usually, such structures are large in size and extend up to the micrometer range [43]. These structures exhibit properties that are different from the ones of the individual particles and require interactions so that a stable equilibrium structure can be formed. To synthesize the dendritic gold nanostructures (gold nanodendrites) in the range for few hundred nanometers a variety of molecules like polyaniline (PANI) [44], catechol-grafted dextran [45], long chain amines [46], are known to provide different interactions between gold nanocrystals and to induce the formation of such structures.

Interestingly in our experiments we found that, when the same amount of L-tyrosine (as above for twisted nanorods) was added to the Au³⁺ solution prior to the addition of citrate, spherical nano-dendritic gold structures entirely made by clumping and entangling of twisted nanorods or small nanowires were obtained (see Supplementary data Fig. S4 a to d, [Au³⁺(1) + L-tyrosine (2) + Trisodium Citrate (3)]). TEM images of the obtained nanostructures are depicted in Fig. S4 (Supplementary data) and further description of this structure is also reported therein. The UV-vis spectra displayed similar flat absorption profiles as for twisted gold nanorods and the change in colour of the solution was the same as observed for twisted nanorods, as discussed above.

We next carried out XPS studies of the twisted nanorods and gold nanodendrites for the investigation of the chemical composition and surface study of gold nanocrystals. Results are reported in Supplementary data.

3.3. Formation mechanism of twisted nanorods

We found out that, by reducing the amount of L-tyrosine in the reaction mixture to about one quarter as compared to the previous article on gold nanoflowers,[24] the morphology of the particles completely changes from 3D nanoflowers to 1-D twisted gold nanorods or gold nanodendrites depending on the sequence of addition of reagents in the reaction mixture i.e. whether tyrosine is added after or before citrate in the gold solution, respectively. When gold solution is mixed with citrate ultra-small gold nanoparticles are formed initially, which fuse together to form nanowire networks [17]. This fusion of gold seeds or ultra-small gold nanoparticles can be prevented by adding polyvinylpyrrolidone (PVP) in the reaction mixture which results in the formation of spherical gold nanoparticles with diameters ≤ 5 nm [38,42]. Here, the addition of L-tyrosine, instead of PVP, somehow also prevents the formation of large 2-D nanowire networks and results in the formation of twisted gold nanorods. Till date there are no articles on homogenous colloidal solution of twisted gold nanorods, while there are very few articles on aqueous-phase room-temperature synthesis of hyper branched dendritic gold nanostructures [47,48]. In order to understand the growth process, time dependent UV-vis spectra were acquired during the formation of twisted nanorods (Fig. 1a). An increase in absorbance with time was observed in the entire wavelength range extending up to the NIR region (Fig. 1a & b). In summary, an induction time was noticed followed by broad absorption profiles and an increase in absorbance in the entire visible–NIR region, with a prominent isosbestic point at around 250 nm. In due course a broad peak was developed at ~ 550 nm which slightly blue shifted during the reaction (Fig. 1a & b). This growth was similar to that seen in our previous articles on gold nanowire network and gold foam [17]. However the main advantage is that now a small structure with nanometer dimensions is displaying the absorption profile of gold nanowire networks [41]. Thus, these gold nanostructures present advantages of both nanorods and nanowires. The colloidal sol was stable and also did not precipitate with time to form gold nanofoam as in the case of our previous studies [17].

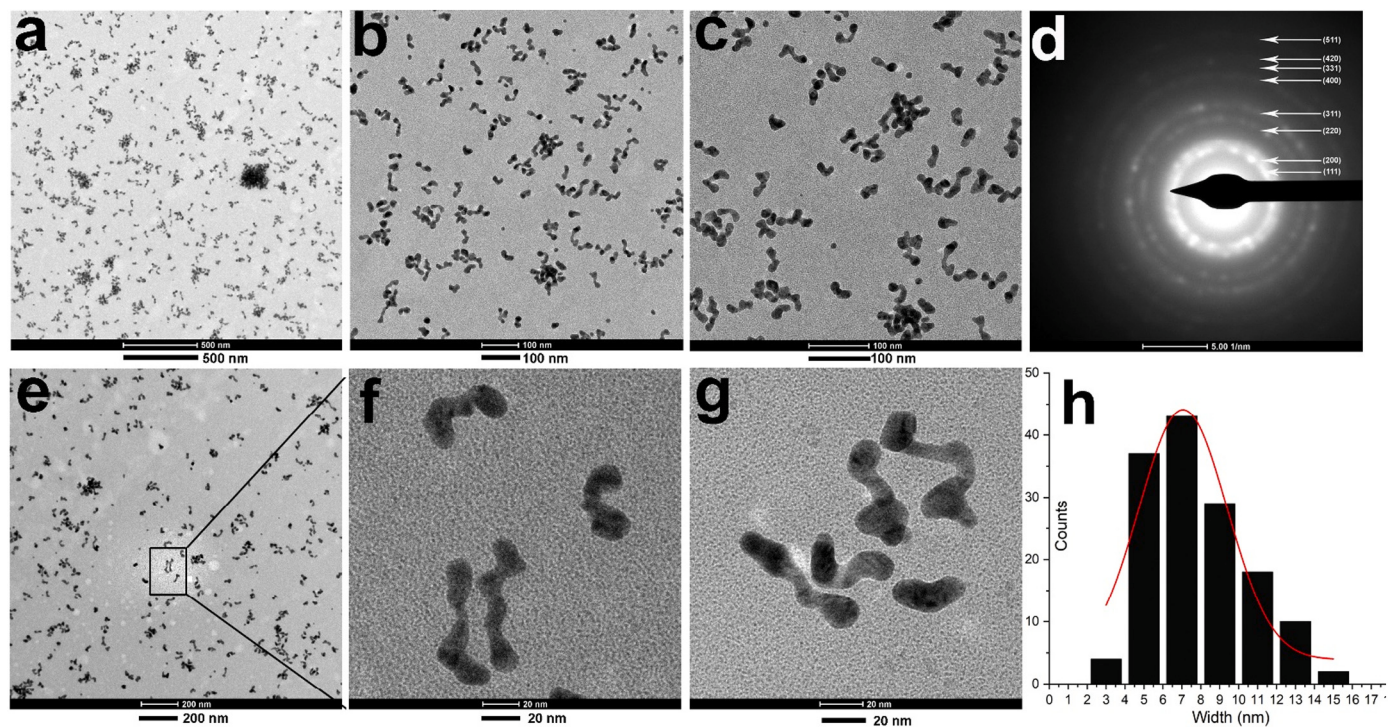


Fig. 2. (a-c & e-g) TEM images of as prepared twisted gold nanorods at different magnifications. (d) SAED pattern of twisted gold nanorods displaying polycrystalline and fcc structure (h)Size distribution histogram of twisted gold nanorods (width). The amount of citrate, L-tyrosine and gold in the final reaction mixture for all samples were citrate = 19.4 mM, Au^{3+} = 2 mM and L-tyrosine = 0.275 mM Sequence of addition of reagents [Au^{3+} + Citrate] + L-tyrosine. (For interpretation of the references to colour in this figure legend, the reader is referred to the web version of this article.)

As discussed in previous articles [24] we believe that when L-tyrosine is added after the addition of citrate, the L-tyrosine molecules have lots of options to interact with, and they interact both with gold ions and citrate molecules and then probably form some sort of self-assembled structures due to the different types of interactions in the reaction mixture. It has been previously reported that L-tyrosine forms a variety of well-ordered self-assembled structures of different shapes depending on the concentration [49,50]. In our previous article [24] we also noted that, when L-tyrosine molecules interacted with citrate first rather than with gold salt, elongated quasi-spherical particles were formed. In that case, L-tyrosine could only modulate the final shape in form of quasi-spherical particles [24]. Here, we believe that due to the insufficient amount of L-tyrosine in the mixture, the amine residues of the tyrosine molecules soon become saturated with gold ions and thus become the limiting factor. L-tyrosine molecules reduce gold ions to atoms and strongly bind with the gold surface, as also revealed by XPS studies (see Supplementary data for details). However, due to their less amount they are only able to reduce a small percentage of gold ions present in solution while most of the Au^{3+} ions are reduced by citrate molecules which now take active part in reduction and prompt the linear growth of gold nuclei formed in the solution, Fig. 3a & b. The linear growth mediated by citrate has been discussed in detail in our previous article [17]. TEM analysis of intermediate structure (Fig. 3c) obtained after 3–4 min of reaction in solution reveals the formation of many small particles which have a size less than 5 nm. After about 7–10 min of reduction process, small clusters of linear particles and small projections from spherical particles could be seen (Fig. 3d). A closer examination of TEM, SAED patterns and AFM images of twisted nanorods supports this theory as the ends of twisted nanorods were rounded and thicker than the middle connecting parts (Fig. 2). At room temperature trisodium citrate has the tendency of modulating the shape of gold nanocrystals in form of nanowire networks [17] however addition of a third molecule in reaction mixture greatly influences the shape of the final material [24,38]. In the present case because of its

low amount, L-tyrosine can only partially modulate the shape of gold nanocrystals, luckily resulting in the formation of a new type of structure, the twisted nanorod.

TEM observation in normal mode provides only a 2-D projection of the morphology, therefore, to visualize their morphology in 3-D, we carried out electron tomography [24] and atomic force microscopy. The twisted nanorods were tilted at different angles relative to the electron beam from 0° to +30°. From the images (Fig. 4a-d) it could be seen that individual particles have a cylindrical structure similar to a wire or a rod rather than a flat structure as a ribbon.

AFM analysis (Fig. 4e & f) gave a clear picture of the particles and revealed that each structure was made up of two spherical or irregular particles connected by a small segment of twisted or bent nanowire. Fig. 4e and f show AFM and high magnification TEM images of a typical twisted nanorod.

It is well known that it is hard to deposit Au onto a specific plane of a nanocrystal once strong ligands are bound onto the gold surface. From the XPS results (see Supplementary data for details) as well as from our previous publication [24] it was obvious that L-tyrosine binds strongly on the surface of gold. In the case of nanoflowers we showed how L-tyrosine overall changed the morphology or final product by blocking trisodium citrate molecules and thus preventing linear growth [17]. However, in the present case due to the very less amount of L-tyrosine some ligand deficient spaces do occur on the gold surface. At these deficient places a dynamic competition drive, force Au ions to the site, where they are reduced by the excess of citrate already present in the solution, thus giving a new surface layer for deposition and reduction of more gold ions. These places thus become sites for citrate reduction and a linear growth occurs most probably by the mechanism described before [17,24]. In summary, with less amount of L-tyrosine small islands remain deficient of L-tyrosine molecules; this island thus grows linearly in length and finally the reaction terminates because of the exhaustion of gold ions or citrate in solution.

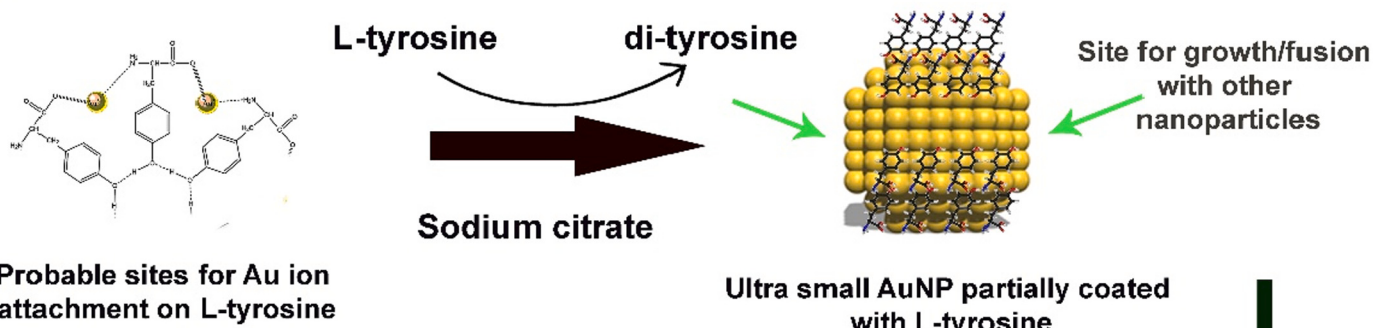
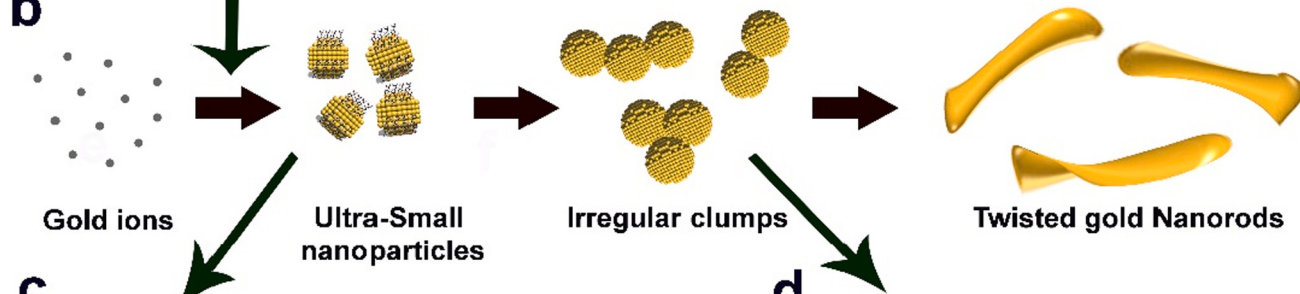
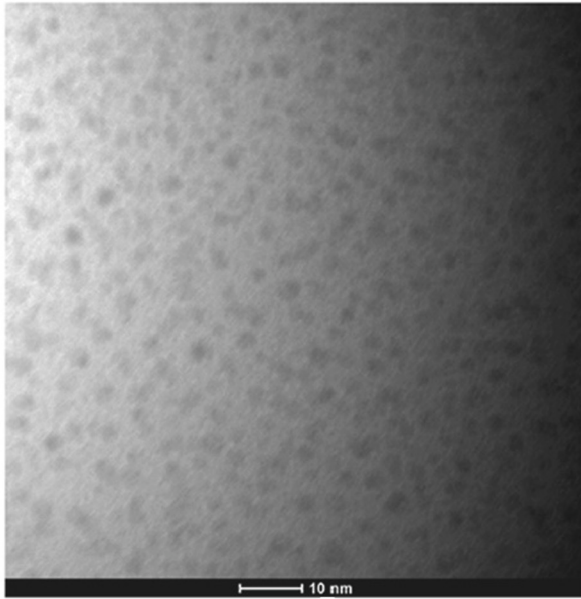
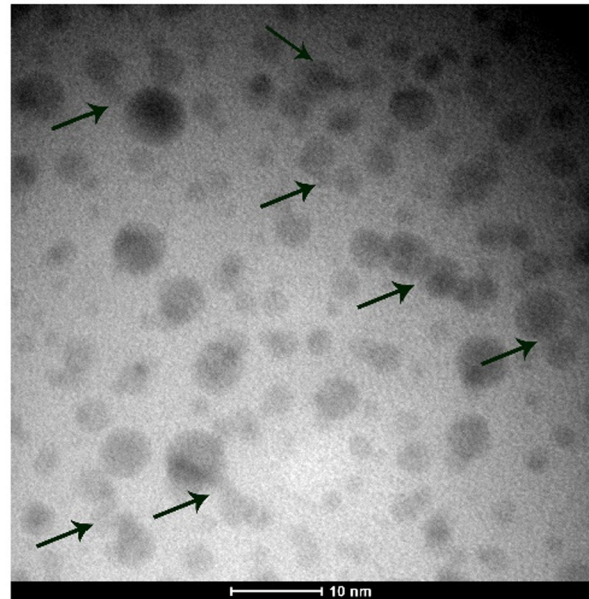
a**b****c****d**

Fig. 3. Scheme for formation of twisted gold nanorods by L-tyrosine and trisodium citrate molecules. (a&b) Interaction of gold ions (shown in yellow) with L-tyrosine, and formation of ultra-small gold nanoparticles. (c) Formation of ultra-small nanoparticles as monitored by TEM. (d) Clumping and growth of nanoparticles as monitored by TEM, when the colour of the solution darkens. Scale bar 10 nm in both micrographs. (For interpretation of the references to colour in this figure legend, the reader is referred to the web version of this article.)

3.4. Theoretical model based on experimental evidence of migration and coalescence of Au nanoparticles (cellular automata and DLA simulations)

We used DLA models to simulate the formation and growth of twisted gold nanorods. DLA (Diffusion Limited Aggregation) is a numerical technique of approximation of natural processes of nucleation and growth, in which the motion of individual particles and the entire system is discretized in finite elements. In the technique, the formation of a structure is the result of the accumulation of smaller building blocks around an initial seed (Fig. 5). In this case, the seed is represented by the L-tyrosine molecules: gold ions resulting from the

dissociation of gold chloride in solution move in the system driven by the sole diffusion until they collide with the seed. Collision is the originating event that allows the randomly moving gold particle to be incorporated by L-tyrosine. The repetition of this hit-and-stick process generates an aggregate of a high number of gold particles, i.e. of the final twisted gold nanorod structure. The method presumes that the motion of individual particles in the domain is stochastic, thus the trajectory of each particle is a random walk (Fig. 5a). Injection of trisodium citrate in the solution (methods) is akin to the inclusion of a damping agent that modulates the speed of formation of the gold nanostructures: its effects can be simulated by changing the probability of

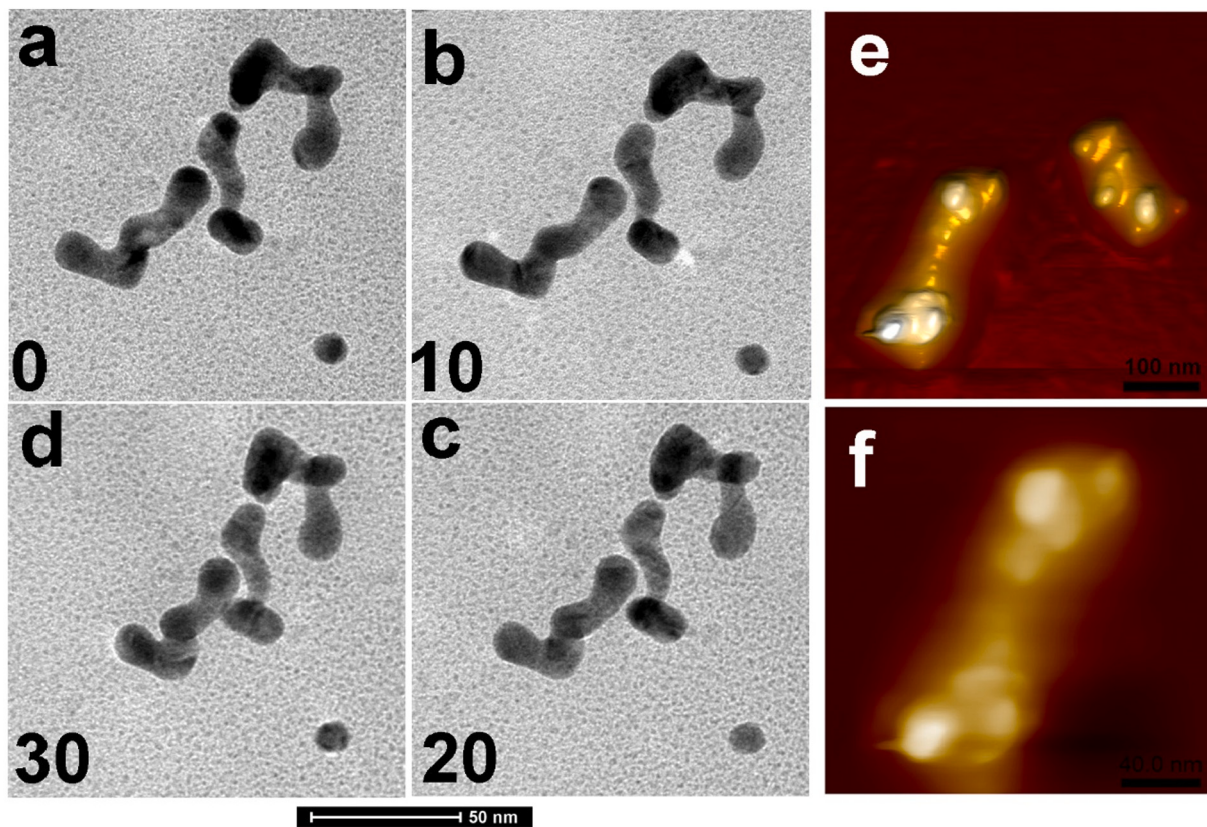


Fig. 4. TEM tomography and AFM analysis of twisted gold nanorods. (a-d) TEM tomography of a twisted gold nanorods at different angles (0 to +30°) to display the 3-D structure. (e, f) AFM images of twisted gold nanorods displaying cylindrical structure. (For interpretation of the references to colour in this figure legend, the reader is referred to the web version of this article.)

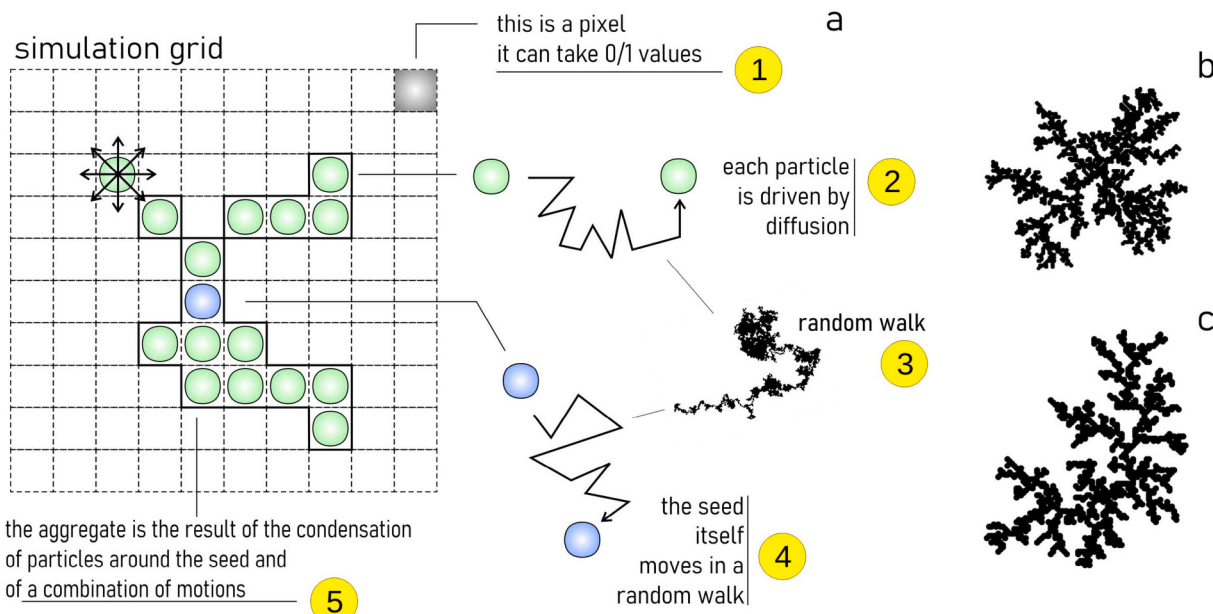


Fig. 5. Numerical simulations of gold nanoparticle growth. In a DLA simulation the system is discretized in a grid: (a) The continuous motion of each particle is approximated as a sequence of fundamental steps, and the aggregate is formed upon accumulation of the particles around a seed. (b) After a large number of repetitions, the process yields an aggregate with a fractal appearance and circular symmetry if the initial seed is fixed in the domain or (c) without any apparent symmetry if the seed is subjected to the Fick's laws of diffusion. (For interpretation of the references to colour in this figure legend, the reader is referred to the web version of this article.)

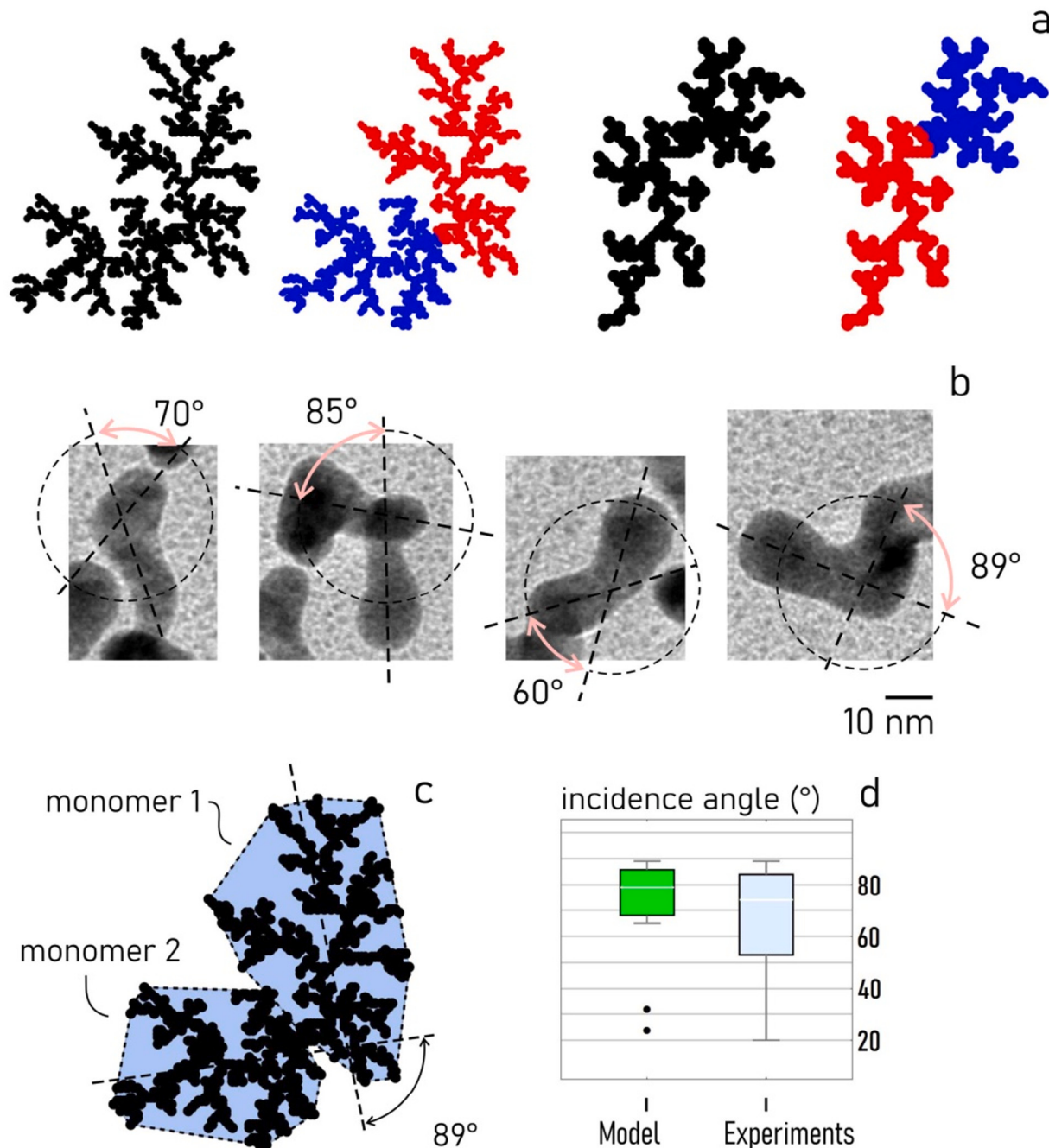


Fig. 6. Analysis of DLA aggregates and comparison with experiments: particle-chain conformation. (a) The final DLA aggregates generated from simulations can be divided into elements with some internal coherence, that we call monomers. (b) Likewise, real twisted gold nanorods are not homogenous, but can be divided into monomers, with a discontinuity arising at the interface between a monomer and another. (c) We calculated the intrinsic angle of each numerical aggregate, determined as the angle between the principal directions of its constituent monomers. (d) The angle predicted by the model is statistically similar to that measured from experiments. (For interpretation of the references to colour in this figure legend, the reader is referred to the web version of this article.)

adhesion of the particle to the aggregate, sp , between 0 and 1. Moreover, since in the present experimental set-up, L-tyrosine is added at the end of sample preparation (methods), we put forward the hypothesis that the position of L-tyrosine (the seed) and of the entire aggregate is not fixed in the domain, but it varies over time tracing, in turn, a random walk. This implies that the final form of the aggregate is a result of the combination of motions. While, with a fixed seed, one obtains an aggregate with circular symmetry (Fig. 5b), if the position of the seed is let free to move, symmetry is broken (Fig. 5c) and the final numerical aggregate shows preferential directions of propagation, resembling real twisted gold nanorods.

In aggregates like those reported, as for an example, in Fig. 5c & Fig. 6a, particles in the aggregate do not develop along a straight line. We subjected each aggregate to a cluster analysis algorithm developed by Alex Rodriguez and Alessandro Laio in reference [51]. The algorithm finds the cluster centers as those points with higher density than their neighbors do and with a relatively large distance from points with higher densities. Upon analysis, we found the emergence in each aggregate of 2 clusters (Fig. 6a), indicating that particles of the aggregate are preferentially distributed in 2 different groups, each of which with a characteristic axis intersecting at an angle that approaches 90°. These topological characteristics of the numerical aggregate turn out to be an

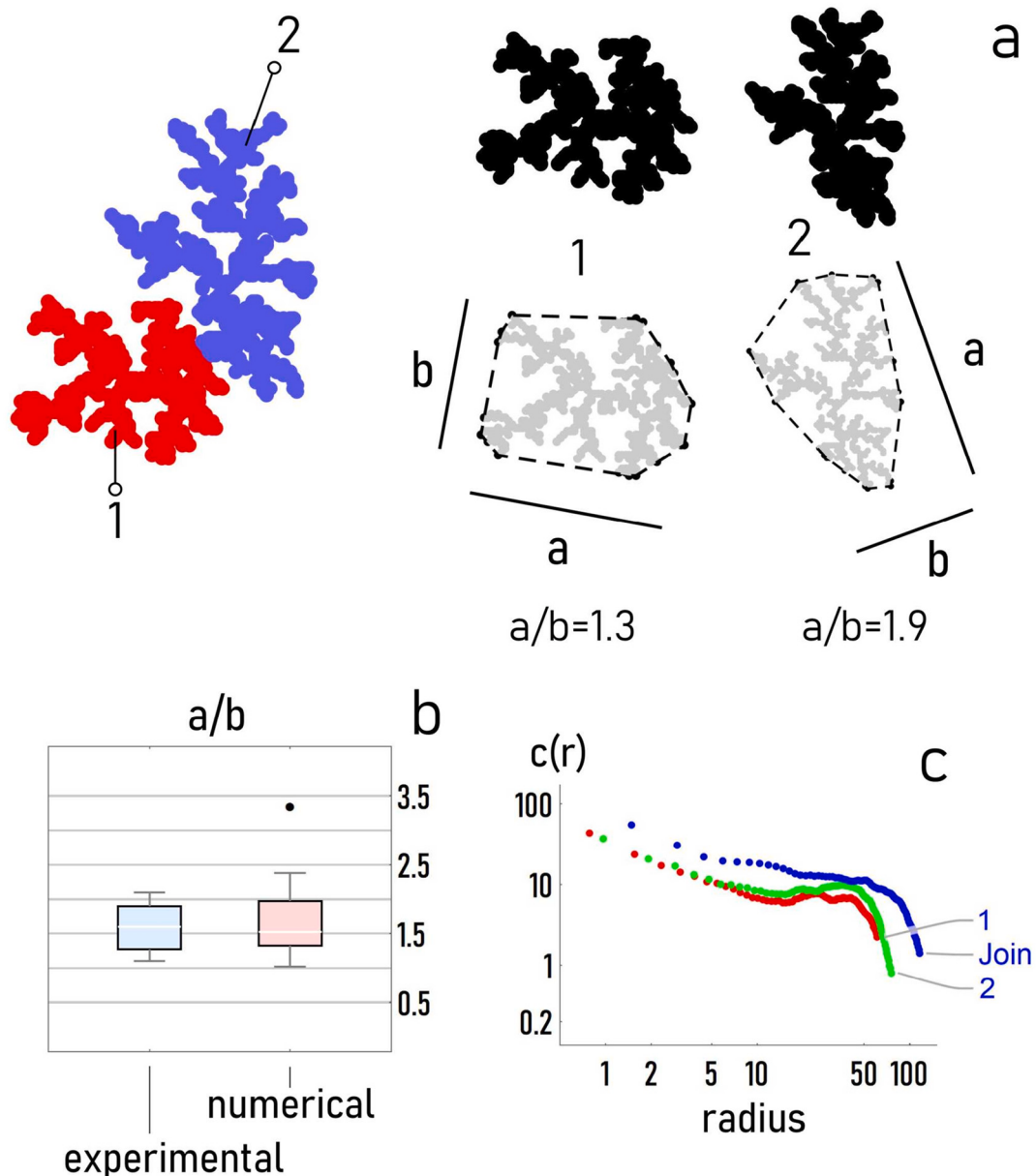


Fig. 7. Analysis of DLA aggregates and comparison with experiments: particle morphology. (a) Each monomer constituting the aggregate has a certain level of slenderness, or factor of form, defined as the ratio between its major to its minor axis, a/b , if $a/b = 1$ the monomer is inscribed in a circle. (b) The factor of form resulting from the simulations is similar to that measured from the experiments, with $a/b > 1.5$. (c) Fourier analysis and the density-density correlation function of the numerical aggregates indicates that the fractal dimension of the structures oscillates around $D_f \sim 1.55$, with small differences between the whole aggregate and each of the monomers.

analogue of the morphological characteristics of the real twisted gold nanorods imaged by transmission electron microscopy (TEM), being these a chain of repeated subunits, or monomers, rotated by a certain angle at the junction between two adjacent monomers (Fig. 6b). To estimate the obedience of the model to the experimental template, for each numerical aggregate: (i) we found the elemental monomers in which it is divided, (ii) we determined the smallest convex polygon that encloses all of the points of the first and of second monomer (i.e. the *convex hull* of those sets). Then, (iii) we found the principal directions of the first and of the second monomer as the eigenvectors of the moment-of-inertia tensor of the points in the sets relative to their center of mass and (iv) we determined the angle α between those principal directions (Fig. 6c). We then compared the tilting angle α predicted by the DLA model to the angle β measured from experiments (Fig. 6d). The model indicates that internal angle of rotation of the aggregate is

$\alpha = 72^\circ \pm 18^\circ$, averaged over more than 30 simulations. At the same time, the internal zigzag angle measured from the gold nanorods is $\beta = 67^\circ \pm 21^\circ$. In this case, β is averaged over more than 4 features extracted from at least 10 nanorods, for a total of more than 40 technical repeats. A Student's *t*-test was performed to test whether the means of the numerical and experimental measured angles are equal: $p - values$ much greater than 0 ($p - value \sim 0.45$), indicate that the means of the two populations are not statistically significantly different from one another and that the DLA template that we used in these trials is a good model for predicting nanorods conformation and configurations.

The aspect ratio or factor of form of each monomer is another morphological characteristic that can be considered to compare the output of the simulations with the experimental results. The factor of form is a proportional relationship between an object's maximum and

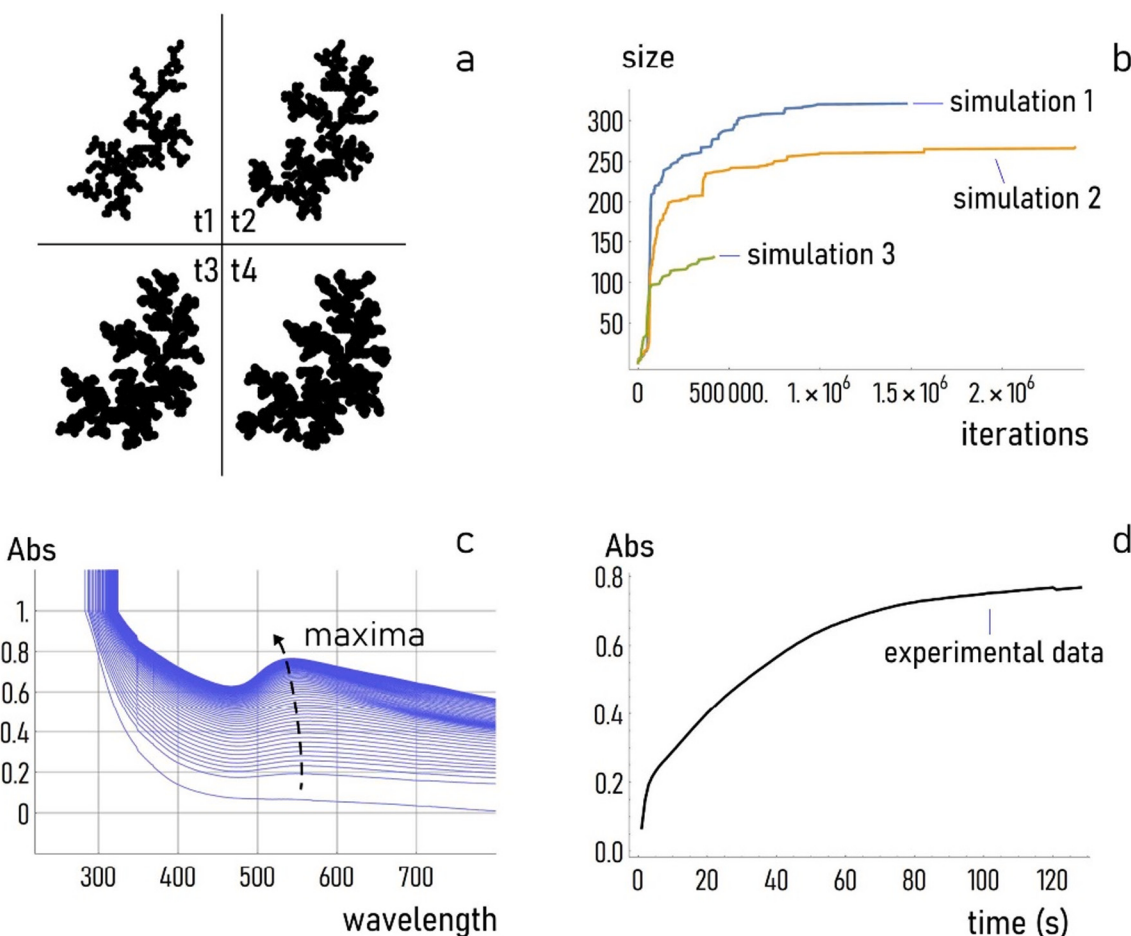


Fig. 8. Predicting particle growth dynamics. (a) Numerical DLA aggregates develop over time, here we show the structure at different numbers of iterations: $t_1 = 20,000$, $t_2 = 50,000$, $t_3 = 100,000$, $t_4 = 1,000,000$. (b) The resulting curve of growth of the aggregate is a negative exponential function evolving towards a steady state value. (c) Analysis of UV spectra of samples enabled to determine the dynamics of formation of twisted gold nanorods: (d) the prediction of the model matches with a very good accuracy with the experimental observations. (For interpretation of the references to colour in this figure legend, the reader is referred to the web version of this article.)

minimum length. In the case of a numerical aggregate, particles of the aggregate can be clustered into groups as described above. Those groups (monomers) are the smallest irreducible building blocks of the aggregate with some internal correlation. For these, one can find their maximum (minimum) length along (perpendicular to) the principal direction of the monomer. We shall call the maximum monomer size a , and the minimum monomer size b . The ratio a/b is a factor of form for that monomer (Fig. 7a). The larger a/b more elongated is the structure. For $a/b = 1$, the monomer is a circle, at the limit of $a/b \rightarrow 0$ or $a/b \rightarrow \infty$, the monomer collapses into a monodimensional line. We calculated the values of a , b , and a/b resulting from more than 30 simulations. We then compared the results to the values of a/b obtained from TEM images of twisted gold nanorods through standard image analysis techniques (Fig. 7b). In this case, the values of a/b were calculated over more than ~ 40 features extracted from the TEM images of the nanorods. We found that the factor of form predicted by the model is $a/b = 1.57 \pm 0.35$, indicating that the numerical monomers are mostly elongated, whereas the factor of form measured from the experimental data is $a/b = 1.76 \pm 0.71$. The difference between the two is not statistically significant: values of p much greater than zero ($p - value \sim 0.41$) indicate that data are consistent with the model. To characterize the topology of the aggregates more accurately, we used the density-density correlation function (Fig. 7d), defined – among others – in reference. The density-density correlation function $c(r)$ correlates the information content of the numerical aggregate (c) to its

length scale r , expressed in pixels, in a bilogarithm plot. The slope (S) of the function in the linear region of the diagram can be used to determine the fractal dimension of the aggregate as $D_f = 2 - S$. The fractal dimension is a number comprised between 1 and 2 (in a 2D geometry) that indicates the change of complexity to the change in scale of a structure. We found that the fractal dimension of the entire aggregate is $D_f \sim 1.58$, compared to marginally different values of fractal dimension $D_f^A \sim 1.52$ and $D_f^B \sim 1.54$ derived for the first and the second monomer in which it is partitioned. Low variability of the fractal dimension values indicates that internal fine structure and topology of each monomer is similar to that of the originating aggregate.

DLA aggregates are generated over time. Fig. 8a shows timeshots of the numerical aggregate after $t_1 = 20,000$, $t_2 = 50,000$, $t_3 = 100,000$, $t_4 = 1,000,000$ of iterations from the beginning of the process. Remarkably, the dynamics of the formation of the system can be described by a negative exponential function of the form $m(t) = m_0(1 - e^{-t/\tau})$, with the mass m of the aggregate varying from zero to the steady state value m_0 (Fig. 8b). In the equation, τ is the time constant, i.e. the time necessary to the system to reach the 66% of its final mass. For the configurations used in Fig. 8a and a sticking probability $sp = 0.5$, we found that $m_0 = 293 \pm 27$ particles and $\tau = 123,000 \pm 11,000$ iterations. Moreover, during the early time of the process, in which the expansion of the system is linear, we found a constant rate of aggregation of $k \sim 3 \times 10^{-3}$ particles/iteration. We used UV analysis of samples (methods) to determine experimentally the dynamics of growth

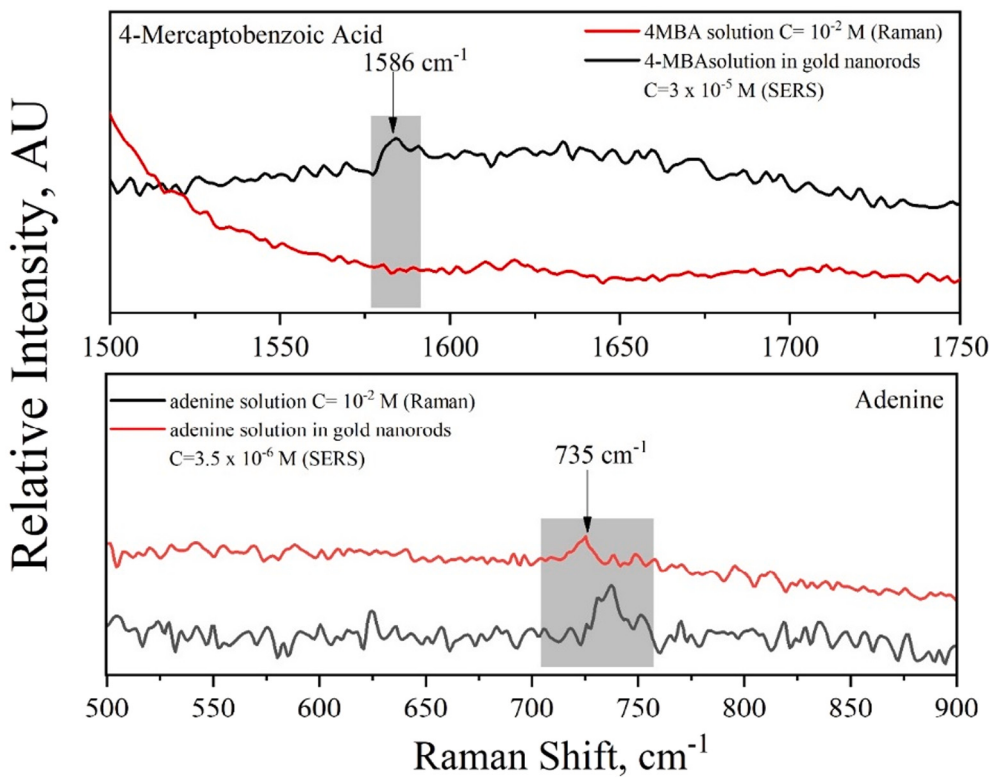


Fig. 9. SERS spectra of (a) 4-MBA and (b) adenine on twisted gold nanorods. (For interpretation of the references to colour in this figure legend, the reader is referred to the web version of this article.)

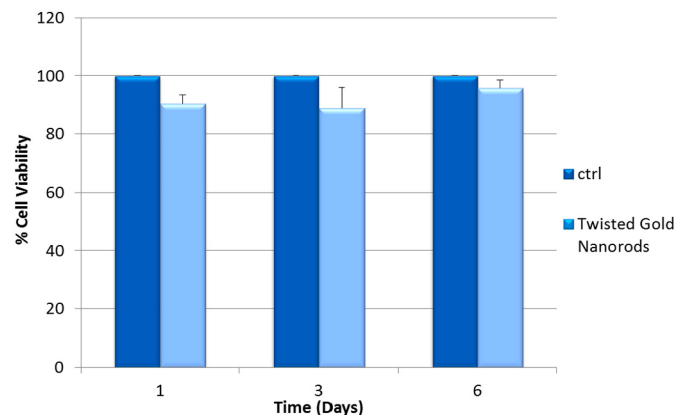


Fig. 10. In vitro cytotoxicity evaluation by means of Alamar Blue Assay of twisted gold nanorods at a final gold concentration of 0.2 mM in bEnd.3 cells. Data were reported as percentage of viable cells normalized to untreated control cell. (For interpretation of the references to colour in this figure legend, the reader is referred to the web version of this article.)

of twisted gold nanorods. The time evolution of the system was determined as the rate of change of the intensity of the peaks found in each of the spectra as a function of time (Fig. 8c). The resulting curve of growth of the nanorods is reported in Fig. 8d. The dynamics of the system that we found for the nanorods is comparable to that which we found using DLA simulations: the prediction of the model matches with the experimental data for several different time intervals. Furthermore, the time constant that we found for the real gold nanorods is $\tau \sim 27$ s that, compared to the one determined numerically, yields a conversion factor of $c \sim 4555$ iterations/s, i.e. approximately 4555 cycles of simulation are equivalent to 1 s of the real physical process.

3.5. Surface Enhanced Raman Scattering

It is well known that gold nanostructures hold unique optical properties and can induce huge enhancement in the Raman scattering (Surface Enhanced Raman Scattering) because of the localized surface plasmons [52]. Twisted gold nanorods have a coarse surface, thus increasing the surface area and forming higher amount of ‘hot spots’ on their surfaces compared to spherical nanoparticles. We therefore tested the proposed gold nanostructures as SERS active substrates. As probe molecules, we focused on adenine [53] and 4-MBA [54], molecules widely used in SERS experiments because both adsorb on gold surface (adenine via the amine group and 4-MBA via the sulfur containing on to the mercapto group). The samples were prepared by mixing the probe molecules with the gold nanostructures. The samples were prepared by mixing the probe molecule with twisted gold nanorods, in a ratio 1:1 v/v to a final volume of 100 μ L. Then 30 μ L of the final solution were dropped on a microscope glass slide covered with aluminum foil while the 780 nm laser line was focused onto the drop with the 10 \times /0.25 LWD objective. Fig. 9 shows that twisted gold nanorods generate SERS spectra with significant enhancement factors, however the enhancement to Raman scattering was much higher for adenine as compared to 4-MBA. More detailed, for both adenine and 4-MBA solutions were detected at a concentration level of 3.5×10^{-6} and 3×10^{-5} respectively, with an enhancement factor of around 10^3 – 10^4 . In Fig. 9, characteristic bands for both adenine and MBA are also presented. For adenine, it was centered at 735 cm^{-1} which is assigned to the ring breathing mode and for MBA the characteristic Raman bands was at 1586 cm^{-1} assigned to the ring stretching mode.

3.6. Cytotoxicity

A nanomaterial to be considered for implementation in biological applications must be tested for its biocompatibility in physiological systems. To assess biocompatibility of the twisted gold nanorods, their

cytotoxic effect was evaluated in vitro on a cell line model (b.End3) by means of Alamar Blue assay. Fig. 10 depicts cell viability percentage of treated cells normalized to non-treated cells. Preliminary data on one cell line show that twisted gold nanorods do not interfere with cell proliferation at any contact time even at high concentrations.

4. Conclusions

In summary we have developed an easy, one pot protocol for the synthesis of a novel structure we have named twisted gold nanorods as well as gold nanodendrites without using any seed mediation, heat, hazardous solvents and toxic molecules. Both the structures are synthesized by the same set of starting reagents and are developed just by manipulating with the sequence of addition of reagents to a solution of auric chloride. For example, adding L-tyrosine prior to citrate results in the formation of dendritic gold nanostructures and adding it after citrate results in separate small sized twisted gold nanorods. We have hypothesized a reasonable mechanism based on our previous studies of gold nanowire networks, and gold nanoflowers [24]. Results of the simulations reproduced convincingly the morphological characteristics of the twisted gold nanorods and the time evolution of the entire system, indicating that the initial hypothesis is correct and providing the theoretical background necessary for the rational design of anisotropic gold nanoparticles. Very interestingly, proposed twisted gold nanorods possess unique absorbing properties extending up to SWIR region with an enormous potential in the field of in vivo photo-thermal applications. By preliminary cytotoxicity tests, we have shown that the twisted gold nanorods are able to be internalized by b.End3 cells in a safe manner at a final gold concentration of 0.2 mM until 6 days of treatment. Finally, we have also assessed SERS activity of twisted gold nanorods.

CRediT authorship contribution statement

- Anshuman Jakhmola: Conceptualization, Methodology, Investigation, Writing - Original Draft.
- Raffaele Vecchione: Conceptualization, Resources, Writing - Original Draft, Writing - Review & Editing, Supervision, Project administration.
- Valentina Onesto: Conceptualization, Methodology, Formal analysis, Writing - Original Draft, Writing - Review & Editing.
- Francesco Gentile: Conceptualization, Methodology, Formal analysis, Writing - Original Draft, Writing - Review & Editing.
- Martina Profeta: Methodology, Investigation, Writing - Original Draft.
- Edmondo Battista: Methodology, Investigation, Writing - Original Draft.
- Anastasios C. Manikas: Methodology, Investigation, Writing - Original Draft.
- Paolo A. Netti: Resources, Supervision, Project administration, Funding acquisition.

Declaration of competing interest

The authors declare that they have no known competing financial interests or personal relationships that could have appeared to influence the work reported in this paper.

Acknowledgements

The authors thank Valentina Mollo, Vincenzo Calcagno and Manlio Colella for the TEM and SEM imaging.

Appendix A. Supplementary data

Supplementary data to this article can be found online. More TEM and SEM images of different samples; SAED patterns; UV-vis spectra of fresh and aged samples; XPS data and results. Supplementary data to this article can be found online at <https://doi.org/10.1016/j.msec.2020.111515>.

References

- [1] D.A. Hanifi, N.D. Bronstein, B.A. Koscher, Z. Nett, J.K. Swabeck, K. Takano, A.M. Schwartzberg, L. Maserati, K. Vandewal, Y. van de Burgt, A. Salleo, A.P. Alivisatos, Redefining near-unity luminescence in quantum dots with photothermal threshold quantum yield, *Science*. 363 (2019) 1199–1202, <https://doi.org/10.1126/science.aat3803>.
- [2] Y. Te Liao, V.C. Nguyen, N. Ishiguro, A.P. Young, C.K. Tsung, K.C.W. Wu, Engineering a homogeneous alloy-oxide interface derived from metal-organic frameworks for selective oxidation of 5-hydroxymethylfurfural to 2,5-furandicarboxylic acid, *Appl. Catal. B Environ.* 270 (2020). doi:<https://doi.org/10.1016/j.apcatb.2020.111805>.
- [3] K. Zhang, T.H. Lee, J.H. Cha, H.W. Jang, J.W. Choi, M. Mahmoudi, M. Shokouhimehr, Metal-organic framework-derived metal oxide nanoparticles@reduced graphene oxide composites as cathode materials for rechargeable aluminum-ion batteries, *Sci. Rep.* 9 (2019). doi:<https://doi.org/10.1038/s41598-019-50156-6>.
- [4] Y. Te Liao, B.M. Matsagar, K.C.W. Wu, Metal-organic framework (MOF)-derived effective solid catalysts for valorization of lignocellulosic biomass, *ACS Sustain. Chem. Eng.* 6 (2018) 13628–13643, <https://doi.org/10.1021/acssuschemeng.8b03683>.
- [5] C.C. Chueh, C.I. Chen, Y.A. Su, H. Konnerth, Y.J. Gu, C.W. Kung, K.C.W. Wu, Harnessing MOF materials in photovoltaic devices: recent advances, challenges, and perspectives, *J. Mater. Chem. A* 7 (2019) 17079–17095, <https://doi.org/10.1039/c9ta03595h>.
- [6] E. Doustkhah, J. Lin, S. Rostamnia, C. Len, R. Luque, X. Luo, Y. Bando, K.C.W. Wu, J. Kim, Y. Yamauchi, Y. Ide, Development of sulfonic-acid-functionalized Mesoporous materials: synthesis and catalytic applications, *Chem. - A Eur. J.* 25 (2019) 1614–1635, <https://doi.org/10.1002/chem.201802183>.
- [7] M.-C. Daniel, D. Astruc, Gold nanoparticles: assembly, supramolecular chemistry, quantum-size-related properties, and applications toward biology, catalysis, and nanotechnology, *Chem. Rev.* 104 (2004) 293–346, <https://doi.org/10.1021/cr030698+>.
- [8] T.S. Lopes, G.G. Alves, M.R. Pereira, J.M. Granjeiro, P.E.C. Leite, Advances and potential application of gold nanoparticles in nanomedicine, *J. Cell. Biochem.* 120 (2019) 16370–16378, <https://doi.org/10.1002/jcb.29044>.
- [9] W. Zhou, X. Gao, D. Liu, X. Chen, Gold nanoparticles for in vitro diagnostics, *Chem. Rev.* 115 (2015) 10575–10636, <https://doi.org/10.1021/acs.chemrev.5b00100>.
- [10] M.S. Draz, H. Shafee, Applications of gold nanoparticles in virus detection, *Theranostics*. 8 (2018) 1985–2017, <https://doi.org/10.7150/thno.23856>.
- [11] R.S. Riley, E.S. Day, Gold nanoparticle-mediated photothermal therapy: applications and opportunities for multimodal cancer treatment, *Wiley Interdiscip. Rev. Nanomedicine Nanobiotechnology*. 9 (2017). doi:<https://doi.org/10.1002/wnnan.1449>.
- [12] W. Li, X. Chen, Gold nanoparticles for photoacoustic imaging, *Nanomedicine*, (2015), <https://doi.org/10.2217/nmm.14.169>.
- [13] A. Jakhmola, N. Anton, T.F. Vandamme, Inorganic nanoparticles based contrast agents for X-ray computed tomography, *Adv. Healthc. Mater.* 1 (2012) 413–431, <https://doi.org/10.1002/adhm.201200032>.
- [14] N. Li, P. Zhao, D. Astruc, Anisotropic gold nanoparticles: synthesis, properties, applications, and toxicity, *Angew. Chem. Int. Ed.* 53 (2014) 1756–1789, <https://doi.org/10.1002/anie.201300441>.
- [15] H. Chen, L. Shao, Q. Li, J. Wang, Gold nanorods and their plasmonic properties, *Chem. Soc. Rev.* 42 (2013) 2679–2724, <https://doi.org/10.1039/C2CS35367A>.
- [16] Z. Fan, M. Bosman, X. Huang, D. Huang, Y. Yu, K.P. Ong, Y.A. Akimov, L. Wu, B. Li, J. Wu, Y. Huang, Q. Liu, C. Eng Ping, C. Lip Gan, P. Yang, H. Zhang, Stabilization of 4H hexagonal phase in gold nanoribbons, *Nat. Commun.* 6 (2015) 7684, <https://doi.org/10.1038/ncomms8684>.
- [17] A. Jakhmola, M. Celentano, R. Vecchione, A. Manikas, E. Battista, V. Calcagno, P.A. Netti, Self-assembly of gold nanowire networks into gold foams: production, ultrastructure and applications, *Inorg. Chem. Front.* 4 (2017) 1033–1041, <https://doi.org/10.1039/C7QI00131B>.
- [18] Y. Lu, J.Y. Huang, C. Wang, S. Sun, J. Lou, Cold welding of ultrathin gold nanowires, *Nat. Nanotechnol.* 5 (2010) 218–224, <https://doi.org/10.1038/NNANO.2010.4>.
- [19] T.K. Sau, C.J. Murphy, Room temperature, high-yield synthesis of multiple shapes of gold nanoparticles in aqueous solution, *J. Am. Chem. Soc.* 126 (2004) 8648–8649, <https://doi.org/10.1021/ja047846d>.
- [20] D.K. Smith, B.A. Korgel, The importance of the CTAB surfactant on the colloidal seed-mediated synthesis of gold nanorods, *Langmuir*. 24 (2008) 644–649, <https://doi.org/10.1021/la703625a>.
- [21] P. Priecel, H. Adekunle Salami, R.H. Padilla, Z. Zhong, J.A. Lopez-Sanchez, Anisotropic gold nanoparticles: preparation and applications in catalysis, *Chin. J. Catal.* 37 (2016) 1619–1650, [https://doi.org/10.1016/S1872-2067\(16\)62475-0](https://doi.org/10.1016/S1872-2067(16)62475-0).
- [22] L. Feng, Z. Xuan, J. Ma, J. Chen, D. Cui, C. Su, J. Guo, Y. Zhang, Preparation of gold nanorods with different aspect ratio and the optical response to solution refractive

- index, *J. Exp. Nanosci.* 10 (2015) 258–267, <https://doi.org/10.1080/17458080.2013.824619>.
- [23] A.P. Leonov, J. Zheng, J.D. Clogston, S.T. Stern, A.K. Patri, A. Wei, Detoxification of gold nanorods by treatment with polystyrenesulfonate, *ACS Nano* 2 (2008) 2481–2488, <https://doi.org/10.1021/nm800466c>.
- [24] A. Jakhmola, R. Vecchione, F. Gentile, M. Profeta, A.C. Manikas, E. Battista, M. Celentano, V. Onesto, P.A. Netti, Experimental and theoretical study of biodirected green synthesis of gold nanoflowers, *Mater. Today Chem.* 14 (2019) 100203, <https://doi.org/10.1016/j.mtchem.2019.100203>.
- [25] S. Mokashi-Punekar, N.L. Rosi, Deliberate introduction of particle anisotropy in helical gold nanoparticle superstructures, *Part. Part. Syst. Charact.* 36 (2019) 1800504, <https://doi.org/10.1002/ppsc.201800504>.
- [26] X. Xu, H. Zhang, B. Liu, J. Yang, One-pot synthesis of corolla-shaped gold nanostructures with (110) planes, *RSC Adv.* 10 (2020) 8286–8290, <https://doi.org/10.1039/dora00715c>.
- [27] T. Sinha, M. Ahmaruzzaman, Indigenous north eastern India fern mediated fabrication of spherical silver and anisotropic gold nanostructured materials and their efficacy for the abatement of perilous organic compounds from waste water-a green approach, *RSC Adv.* 6 (2016) 21076–21089, <https://doi.org/10.1039/c5ra26124d>.
- [28] Y. Tian, H.V. Zhang, K.L. Kiick, J.G. Saven, D.J. Pochan, Fabrication of one- and two-dimensional gold nanoparticle arrays on computationally designed self-assembled peptide templates, *Chem. Mater.* 30 (2018) 8510–8520, <https://doi.org/10.1021/acs.chemmater.8b03206>.
- [29] I. Chakraborty, W.J. Parak, Protein-induced shape control of noble metal nanoparticles, *Adv. Mater. Interfaces* 6 (2019) 1801407, <https://doi.org/10.1002/admi.201801407>.
- [30] K.Y. Tomizaki, S. Wakizaka, Y. Yamaguchi, A. Kobayashi, T. Imai, Ultrathin gold nanoribbons synthesized within the interior cavity of a self-assembled peptide nanoarchitecture, *Langmuir*. 30 (2014) 846–856, <https://doi.org/10.1021/la4044649>.
- [31] C.-D. Chen, Y.-T. Yeh, C.R.C. Wang, The fabrication and photo-induced melting of networked gold nanostructures and twisted gold nanorods, *J. Phys. Chem. Solids* 62 (2001) 1587–1597, [https://doi.org/10.1016/S0022-3697\(01\)00098-1](https://doi.org/10.1016/S0022-3697(01)00098-1).
- [32] P. Wang, M. Liu, G. Gao, S. Zhang, H. Shi, Z. Li, L. Zhang, Y. Fang, From gold nanorods to nanodumbbells: a different way to tailor surface plasmon resonances by a chemical route, *J. Mater. Chem.* 22 (2012) 24006–24011, <https://doi.org/10.1039/c2jm33330a>.
- [33] B. Lim, P.H.C. Camargo, Y. Xia, Mechanistic study of the synthesis of Au nanotadpoles, nanokites, and microplates by reducing aqueous HAuCl₄ with poly(vinyl pyrrolidone), *Langmuir*. 24 (2008) 10437–10442, <https://doi.org/10.1021/la801803z>.
- [34] C.-J. Huang, P.-H. Chiu, Y.-H. Wang, C.-F. Yang, S.-W. Feng, Electrochemical formation of crooked gold nanorods and gold networked structures by the additive organic solvent, *J. Colloid Interface Sci.* 306 (2007) 56–65, <https://doi.org/10.1016/j.jcis.2006.10.009>.
- [35] Y. Cai, Z. Wei, C. Song, C. Tang, W. Han, X. Dong, Optical nano-agents in the second near-infrared window for biomedical applications, *Chem. Soc. Rev.* 48 (2019) 22–37, <https://doi.org/10.1039/C8CS00494C>.
- [36] Y. Kenry, B. Duan, Liu, recent advances of optical imaging in the second near-infrared window, *Adv. Mater.* 30 (2018) 1802394, <https://doi.org/10.1002/adma.201802394>.
- [37] A. Plan Sangnier, R. Aufaure, S. Cheong, L. Motte, B. Palpant, R.D. Tilley, E. Guenin, C. Wilhelm, Y. Lalatonne, Raspberry-like small multicore gold nanostructures for efficient photothermal conversion in the first and second near-infrared windows, *Chem. Commun.* 55 (2019) 4055–4058, <https://doi.org/10.1039/C8CC09476D>.
- [38] M. Celentano, A. Jakhmola, M. Profeta, E. Battista, D. Guarneri, F. Gentile, P.A. Netti, R. Vecchione, Diffusion limited green synthesis of ultra-small gold nanoparticles at room temperature, *Colloids Surfaces A Physicochem. Eng. Asp.* 558 (2018) 548–557, <https://doi.org/10.1016/j.colsurfa.2018.09.030>.
- [39] Y. Wang, B. Yan, L. Chen, SERS tags: novel optical Nanoprobes for bioanalysis, *Chem. Rev.* 113 (2013) 1391–1428, <https://doi.org/10.1021/cr300120g>.
- [40] S. Li, Z. Kang, N. Li, H. Jia, M. Liu, J. Liu, N. Zhou, W. Qin, G. Qin, Gold nanowires with surface plasmon resonance as saturable absorbers for passively Q-switched fiber lasers at 2 μm, *Opt. Mater. Express.* 9 (2019) 2406, <https://doi.org/10.1364/ome.9.002406>.
- [41] R. Takahata, S. Yamazoe, K. Koyasu, T. Tsukuda, Surface plasmon resonance in gold ultrathin nanorods and nanowires, *J. Am. Chem. Soc.* 136 (2014) 8489–8491, <https://doi.org/10.1021/ja503558c>.
- [42] M. Celentano, A. Jakhmola, R. Vecchione, Irreversible photo-Fenton-like triggered agglomeration of ultra-small gold nanoparticles capped with crosslinkable materials, *Nanoscale Adv.* 1 (2019) 2146–2150, <https://doi.org/10.1039/c8na00353j>.
- [43] Z.-Y. Lv, A.-Q. Li, Y. Fei, Z. Li, J.-R. Chen, A.-J. Wang, J.-J. Feng, Facile and controlled electrochemical route to three-dimensional hierarchical dendritic gold nanostructures, *Electrochim. Acta* 109 (2013) 136–144, <https://doi.org/10.1016/j.electacta.2013.07.123>.
- [44] M. Pan, S. Xing, T. Sun, W. Zhou, M. Sindoro, H.H. Teo, Q. Yan, H. Chen, 3D dendritic gold nanostructures: seeded growth of a multi-generation fractal architecture, *Chem. Commun.* 46 (2010) 7112, <https://doi.org/10.1039/c0cc00820f>.
- [45] H.Y. Son, K.R. Kim, C.A. Hong, Y.S. Nam, Morphological evolution of gold nanoparticles into nanodendrites using catechol-grafted polymer templates, *ACS Omega*. 3 (2018) 6683–6691, <https://doi.org/10.1021/acsomega.8b00538>.
- [46] P. Qiu, M. Yang, X. Qu, Y. Huai, Y. Zhu, C. Mao, Tuning photothermal properties of gold nanodendrites for in vivo cancer therapy within a wide near infrared range by simply controlling their degree of branching, *Biomaterials*. 104 (2016) 138–144, <https://doi.org/10.1016/j.biomaterials.2016.06.033>.
- [47] Y. Shin, C. Lee, M.-S. Yang, S. Jeong, D. Kim, T. Kang, Two-dimensional hyper-branched gold nanoparticles synthesized on a two-dimensional oil/water interface, *Sci. Rep.* 4 (2015) 6119, <https://doi.org/10.1038/srep06119>.
- [48] D. Huang, X. Bai, L. Zheng, Ultrafast preparation of three-dimensional dendritic gold nanostructures in aqueous solution and their applications in catalysis and SERS, *J. Phys. Chem. C* 115 (2011) 14641–14647, <https://doi.org/10.1021/jp2037284>.
- [49] S. Uyaver, H.W. Hernandez, M. Gokhan Habiboglu, Self-assembly of aromatic amino acids: a molecular dynamics study, *Phys. Chem. Chem. Phys.* 20 (2018) 30525–30536, <https://doi.org/10.1039/c8cp06239k>.
- [50] C. Ménard-Moyon, V. Venkatesh, K.V. Krishna, F. Bonachera, S. Verma, A. Bianco, Self-assembly of tyrosine into controlled supramolecular nanostructures, *Chem. - A Eur. J.* 21 (2015) 11681–11686, <https://doi.org/10.1002/chem.201502076>.
- [51] A. Rodriguez, A. Laio, Clustering by fast search and find of density peaks, *Science* (80-.). 344 (2014) 1492–1496. doi:<https://doi.org/10.1126/science.1242072>.
- [52] F. Tian, F. Bonnier, A. Casey, A.E. Shanahan, H.J. Byrne, Surface enhanced Raman scattering with gold nanoparticles: effect of particle shape, *Anal. Methods* 6 (2014) 9116–9123, <https://doi.org/10.1039/c4ay02112f>.
- [53] F. Madzharova, Z. Heiner, M. Gühlike, J. Kneipp, Surface-enhanced hyper-Raman spectra of adenine, guanine, cytosine, thymine, and uracil, *J. Phys. Chem. C* 120 (2016) 15415–15423, <https://doi.org/10.1021/acs.jpcc.6b02753>.
- [54] S. Zhu, C. Fan, J. Wang, J. He, E. Liang, M. Chao, Realization of high sensitive SERS substrates with one-pot fabrication of Ag–Fe 3 O 4 nanocomposites, *J. Colloid Interface Sci.* 438 (2015) 116–121, <https://doi.org/10.1016/j.jcis.2014.09.015>.